J. Fluid Mech. (1990), *vol.* 219, *pp.* 531–544
Printed in Great Britain

Molecular mixing via jets in confined volumes

By R. E. BREIDENTHAL†, V. R. BUONADONNA AND M. F. WEISBACH

Boeing Aerospace & Electronics, Seattle, WA 98124, USA

(Received 18 November 1988 and in revised form 2 January 1990)

A simple model is proposed to describe the molecular mixing characteristics of a two-dimensional turbulent jet that is discharged into a confined volume. The model, which is based on similarity and physical considerations of only the large-scale motions, derives the characteristic time for the problem and identifies the regime for which the mixing will be most rapid. Results are reported for experiments where helium and helium/argon mixtures were injected into a cylindrical volume initially containing air. Using an aspirating probe that measured transient helium concentrations in the volume, the mixing time was determined as a function of the size of the confining volume and the injection parameters. The experimental results are in general accord with the model, and validate the use of the model for the determination of the minimum mixing time.

1. Introduction

Pulsed chemical lasers require two reactive fluids to be brought together and mixed sufficiently rapidly so that they do not prematurely react before the laser pulse is initiated. Not only must the mixing be rapid, but it must be complete enough so that the mixture is adequately uniform for the laser beam to form and to propagate without excessive optical distortion. These constraints place a premium on rapid and uniform mixing. Most internal combustion processes where fuels and oxidizers must be mixed together also require rapid and uniform mixing.

For a system in which a strong chemical reaction occurs, mechanisms such as propellers to stir the two fluids together are generally not practical. An alternative approach is to rely on the injection process itself to stir the fluids. It is possible to inject one or both reactants through a symmetric array of nozzles into a circular cylinder as sketched in figure 1(*a*); Hartung & Hiby (1972) measured the mixing in a steady flow version of this geometry, making axial measurements of mixing for turbulent flow along a tube. In this case, the independent variable is space instead of time. The mixing rate, while high in the near field, soon declines in the far field because the symmetry of the injection geometry precludes any strong, residual, large-scale circulation. However, if the injection geometry is not symmetric, as in figure 1(*b*), a large-scale residual circulation can be expected to persist, thus stirring the mixture continually, even in the far field. Edwards, Sherman & Breidenthal (1985) demonstrated that the mixing rate is maintained at a higher level in the far field with the non-symmetric injection of figure 1(*b*).

The practical advantages of such an approach have been demonstrated in chemically reacting systems; using this injection geometry, Dreiling (1987) has achieved sufficiently rapid mixing to avoid prereactions in fluorine–deuterium laser mixtures that were previously unstable using other mixing techniques.

† Also affiliated with University of Washington, Seattle, WA 98195, USA.

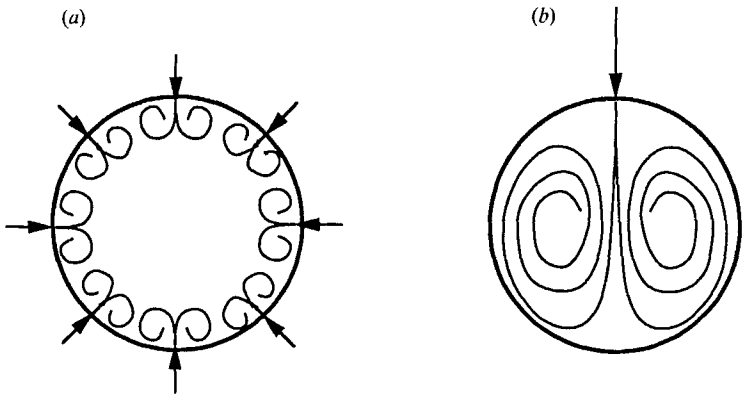

FIGURE 1. Injection strategies: (a) symmetric injection; (b) non-symmetric injection.

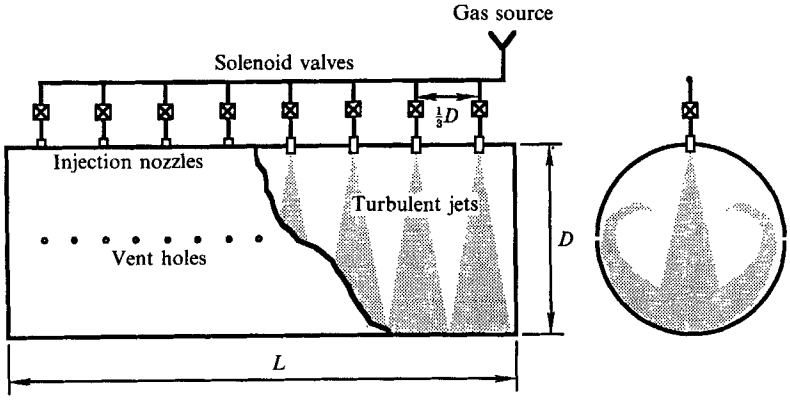

FIGURE 2. Schematic of experimental set-up and flow geometry.

This mixing strategy may also have applications in the chemical process industry. Conventional mixer geometries often consist of many small parallel jets issuing from an array of tubes (Hill 1976), but this approach has no provision for generating large-scale circulation in order to ensure the global uniformity of the mixture.

In this paper we study the temporal problem of one fluid momentarily injected through a linear array of circular nozzles into another fluid already residing in a confined cylindrical volume, as illustrated in figure 2. We are interested in determining the minimum mixing time for cylinders of different diameters and for various fluids (both injected fluid and the final mixture). A model has been developed to achieve this end, and experiments have been carried out that both support the validity of the model and permit determination of the values of the empirical constants used in the analysis.

2. Mixing theory

2.1. *Background*

Molecular-scale mixing ultimately occurs via molecular diffusion across the smallest concentration scales. However, the magnitude of the molecular diffusivity coefficient has a remarkably weak effect on the amount of turbulent mixing (Breidenthal 1981; and Koochesfahani & Dimotakis 1986); the primary factor is the motion of the large-

scale global vortices (Konrad 1976). For example, a factor of 10^3 variation in Schmidt number only changes the amount of turbulent mixing in a plane shear layer by at most a factor of two. Physical reasons for this behaviour have been proposed as follows. The timescale of the largest eddies is much greater than that of all processes at the smallest scales (Marble & Broadwell 1977). It follows that the rate-limiting process is the large-eddy rotation. The weak, residual effect of diffusivity is explained in terms of a flame sheet model, where some of the mixed fluid resides in a thin, diffusive sheet (Marble & Broadwell 1977; Broadwell & Breidenthal 1982). The flame sheet thickness, and hence the amount of mixed fluid within the flame sheet, depends on the molecular diffusivity. However, mixed fluid also resides in larger scale, quasi-homogeneous regions, which are themselves the result of a merging of flame sheets. The amount of mixed fluid in these large-scale regions is independent of diffusivity. Thus only a fraction of all the mixed fluid resides in a thin flame sheet at any instant, and therefore the influence of diffusivity on the total amount of mixed fluid is weak.

The effects of Reynolds number on mixing rates in turbulent shear layers were investigated experimentally (Broadwell & Mungal 1988) and found to be weak for values greater than $\sim 10^4$. Analysis of the flame sheet model (Broadwell & Breidenthal 1982) also concluded that Reynolds-number effects were small for sufficiently large values of Reynolds number. This weak dependency of Reynolds number on mixing rates is consistent with the above discussion on Schmidt-number and fine-scale motion effects. It is therefore sufficient to consider only the large-scale global motions of the fluid to postulate a first-order model for turbulent molecular mixing for the case of interest.

2.2. *Self-similar mixing*

The flow is assumed to be approximately two-dimensional. Quiescent fluid of density ρ initially fills a cylindrical volume of length L and internal diameter D. Along the top of the volume, another fluid is injected through a row of identical, equally spaced nozzles for an injection period t_j (see figure 2). The average nozzle thrust per unit length of the tube is T. This short list of parameters can be used to formulate a theory for the self-similarity of the turbulent mixing process.

When fluid is injected into a confined volume, the largest vortices grow until they fill the entire volume, after which (if the injection is over) no pure fluid remains. In the analysis to follow, we postulate the simplest possible assumption: the mixing and the turbulence are both self-similar.

Self-similar mixing of confined vortices implies that the concentration fluctuations decline by a constant factor at each effective vortex rotation. We further assume that this factor is the natural logarithm base e. Therefore

$$\frac{c'}{\bar{c}} = \mathrm{e}^{-n}, \tag{1}$$

where c' and $\bar{c}$ are the r.m.s. fluctuating and mean concentrations of an inert scalar respectively. n is the effective number of global vortex revolutions occurring after the pure fluid supply has been exhausted; it is the integral of the effective rotation rate,

$$n(t) = \int_{1/\Omega_i}^{t} \Omega(t')\,\mathrm{d}t', \tag{2}$$

where Ω_i is the initial value of the effective rotation rate, Ω, when the vortices first fill the cylinder.

2.3. *Self-similar turbulence*

Self-similar turbulence implies that there is no externally imposed timescale on the flow. Therefore, the only relevant timescale available to the global vortices is their chronological age t (Broadwell & Breidenthal 1982). The effective vortex rotation rate Ω then must be proportional to $1/t$. We further assume that the proportional coefficient is unity. Therefore

$$\Omega(t) = \frac{1}{t}. \tag{3}$$

Evidence to support the assumptions used in deriving (1) and (3) has been obtained in earlier experiments of the analogous spatial problem of transverse jets in ducts (Edwards *et al.* 1985; Breidenthal *et al.* 1986). The explicit dependence of the concentration fluctuations on time is obtained by combining (1)–(3),

$$\frac{c'}{\bar{c}} = \frac{1}{\Omega_i t}. \tag{4}$$

This equation describes the rate at which homogenization of the gas mixture occurs after the initial rotation rate is established.

2.4. *The initial vortex rotation rate*

Following the arguments of Broadwell & Breidenthal (1984), if the injection period is sufficiently short compared to the convection time across the volume, the total impulse per unit length I determines the resulting flow. The impulse is the time integral of the thrust, which for constant thrust is given by

$$I = Tt_j. \tag{5}$$

Besides the jet impulse, the only other parameters of the problem are the cylindrical volume diameter D and initial density ρ of the fluid in it. Using these variables, an initial vortex rotation rate Ω_i can be determined to within a dimensionless constant K_1:

$$\Omega_i = K_1 \Omega_s, \quad \Omega_s t_j \ll 1. \tag{6}$$

Here Ω_s is the characteristic rotation rate for short injection times. From the physical parameters of this problem discussed above, dimensional considerations yield

$$\Omega_s = \frac{I}{\rho D^3}. \tag{7}$$

The greater the jet impulse, the greater the initial vortex spin rate Ω_i. The time it takes for this initial vortex to rotate will be proportional to $1/\Omega_s$.

For long injection times, the jets inject fluid into the vortices during the course of many rotations after the vortices have grown to fill the volume. Since a steady state is achieved, the steady-state vortex rotation rate is determined by the steady-state jet thrust rather than its impulse. In the limit of long injection times, the initial rotation rate Ω_i is proportional to a characteristic long pulse rotation rate, Ω_l.

$$\Omega_i = K_2 \Omega_l, \quad \Omega_l t_j \gg 1, \tag{8}$$

where

$$\Omega_l = \left(\frac{T}{\rho D^3}\right)^{\frac{1}{2}} \tag{9}$$

from dimensional arguments. The greater the jet thrust, the greater the spinning rate of the vortices at the instant the injection is complete.

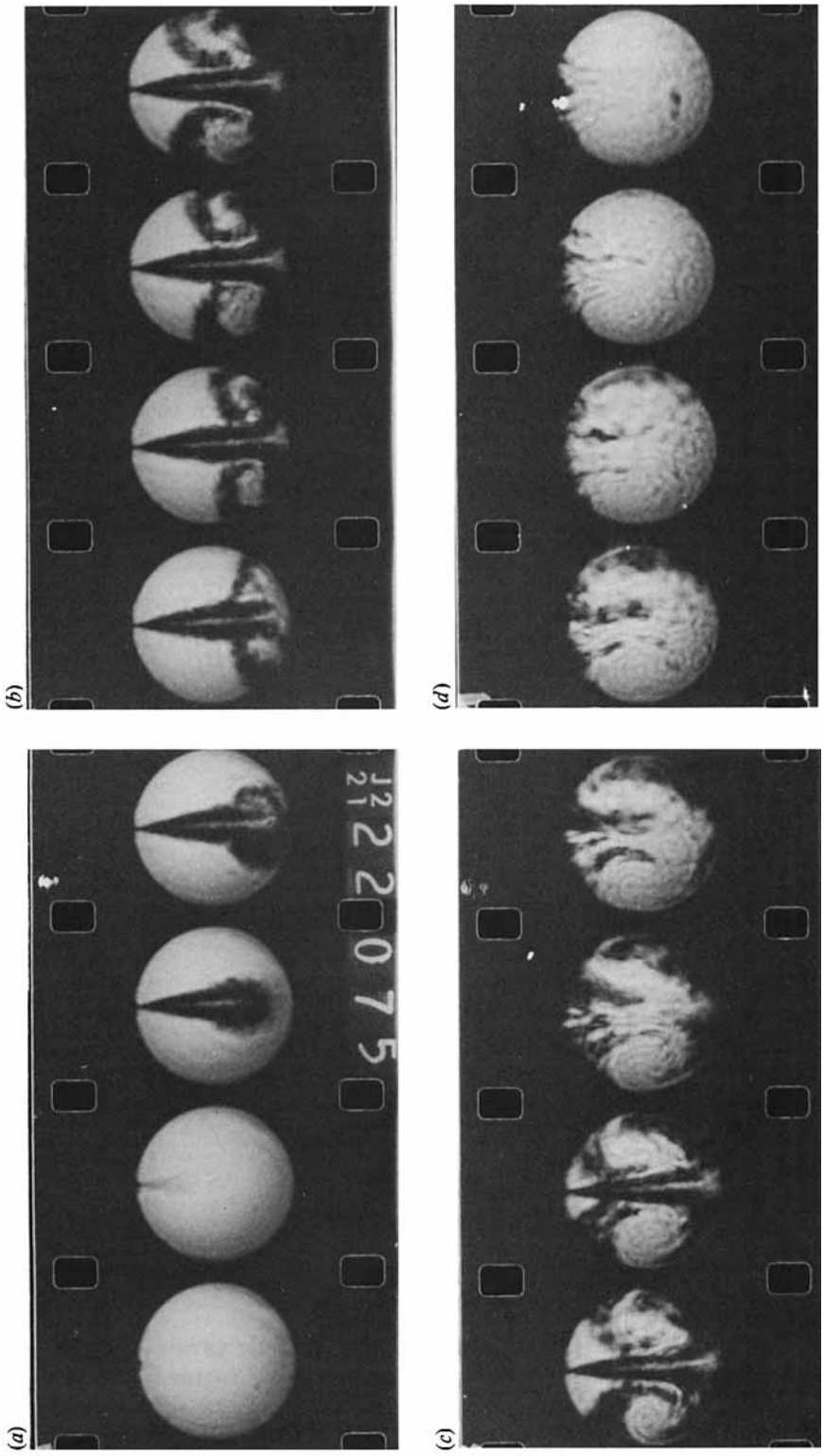

FIGURE 3. Schlieren flow visualization of mixing in a 25 cm diameter cylindrical volume. Time interval between movie frames is $\frac{1}{24}$ s.

2.5. *Mixing times*

Based on the above equations for the initial rotation rates, it is now possible to write the theoretical mixing rate for the two limits of short and long pulse injection. We are interested in the total mixing time, t_{mix}, from the beginning of injection to the instant the fluids are mixed to a specified level of uniformity $c'/\bar{c}$. t_{mix} is the measurable parameter of interest in practical mixing devices. For the short-pulse limit, t_{mix} is just the initial vortex spin up time K_3/Ω_{s}, plus the homogenization time from (4) and (6); so

$$t_{\mathrm{mix}} = \frac{K_3}{\Omega_{\mathrm{s}}} + \frac{1}{(c'/\bar{c})_{\mathrm{s}} K_1 \Omega_{\mathrm{s}}}, \quad \Omega_{\mathrm{s}} t_{\mathrm{j}} \ll 1, \tag{10}$$

and $(c'/\bar{c})_{\mathrm{s}}$ is the specified level of mixing.

For the long-pulse case, the vortices have grown to fill the volume well before the jets are turned off. Therefore, the total time the two fluids are in contact before mixing is just the injection pulse period t_{j} plus the time to mix the fluids after the injection is over, as given by (4), (8), and (9). Thus

$$t_{\mathrm{mix}} = t_{\mathrm{j}} + \frac{1}{(c'/\bar{c})_{\mathrm{s}} K_2 \Omega_1}, \quad \Omega_1 t_{\mathrm{j}} \gg 1. \tag{11}$$

Note that t_{mix} can never be less than t_{j}, and approaches it as Ω_1 increases.

Inserting the appropriate initial rotation rates as defined in (6) and (8), the mixing time is given by

$$t_{\mathrm{mix}} = \begin{cases} \left(K_3 + \dfrac{1}{(c'/\bar{c})_{\mathrm{s}} K_1}\right)\left(\dfrac{\rho D^3}{T t_{\mathrm{j}}}\right), & t_{\mathrm{j}}^2 \ll \dfrac{\rho D^3}{T}, \\ t_{\mathrm{j}} + \left(\dfrac{1}{(c'/\bar{c})_{\mathrm{s}} K_2}\right)\left(\dfrac{\rho D^3}{T}\right)^{\frac{1}{2}}, & t_{\mathrm{j}}^2 \gg \dfrac{\rho D^3}{T}. \end{cases} \tag{12}$$

Examination indicates a characteristic time

$$t_{\mathrm{c}} = \left(\frac{\rho D^3}{T}\right)^{\frac{1}{2}} \tag{13}$$

equal to $1/\Omega_1$. Normalizing (12) by t_{c} and setting $K_3 + 1/(c'/\bar{c})_{\mathrm{s}} K_1 = K_4$ and $1/(c'/\bar{c})_{\mathrm{s}} K_3 = K_5$ yields

$$\tau_{\mathrm{mix}} = \begin{cases} K_4 \dfrac{1}{\tau_{\mathrm{j}}}, & \tau_{\mathrm{j}}^2 \ll 1, \\ \tau_{\mathrm{j}} + K_5, & \tau_{\mathrm{j}}^2 \gg 1, \end{cases} \tag{14}$$

where

$$\tau_{\mathrm{j}} = t_{\mathrm{j}}/t_{\mathrm{c}} \tag{15}$$

and

$$\tau_{\mathrm{mix}} = t_{\mathrm{mix}}/t_{\mathrm{c}} \tag{16}$$

are dimensionless injection and mixing times, respectively.

The above results show that the dimensionless mixing time varies inversely with the dimensionless injection time in the short injection pulse regime, and increases linearly with it for long injection pulses. Furthermore, these relatively simple equations require the determination of only two empirical constants, K_4 and K_5, in order to quantify the mixing rate.

3. Experimental results

The experiment, illustrated in figure 2, consisted of injecting helium or helium/argon gas mixtures into a close cylindrical tube initially filled with air at atmospheric pressure. Two cylindrical tubes of 61 and 91 cm diameter, both having a length of 183 cm were tested. The gas was injected through a single row of nozzles which consisted of simple bulkhead-type gas fittings equipped with cap ends into which an orifice was drilled. Each nozzle had a solenoid valve immediately upstream to control the injection time. Care was taken to ensure that the flow rate, simultaneity and injection time of each valve were identical. A simple gas blowdown system was used for the gas supply. Near-two-dimensional behaviour for the largest scales of the injection process was assured by spacing the nozzles every $\frac{1}{3}D$, which was small enough that the individual turbulent jets could merge together before impinging on the opposite wall. The injection nozzles were operated with either sonic or subsonic conditions at the nozzle orifices. The mass flow rates and thrust of the nozzles were varied by over a factor of 4, and the injection time ranged from 0.2 to 10 s which resulted in injecting as much as 20% by volume into the cylindrical vessels. The characteristic times, t_c, varied from 0.1 to 1.0 s. The Reynolds number, based on a characteristic global velocity D/t_c and scale size D, ranged from 2×10^4 to 5×10^5. Uniformly spaced vent holes along both sides of the cylindrical tubes allowed the experiments to be performed at constant pressure in order to avoid compressive heating effects, since changes in both pressure and temperature affected the probes used for measuring the gas mixedness. For convenience, air was used as the initial gas in the tubes. Before each test, the volume was flushed with air, and a stilling time of several minutes allowed for any residual velocity from the flushing to decay.

3.1. *Flow visualization*

A 25 cm diameter version of our mixing apparatus was duplicated at Los Alamos National Laboratory, where flow patterns were observed with schlieren photography. Figure 3 is a sequence of photographs showing the vortex pair from the starting jet. Note that at the instant of impingement on the bottom wall, the vortex pair is small compared with the cylinder diameter, so that most of the fluid initially in the cylinder remains unmixed. The vortex pair continues to grow as it reverses, eventually engulfing the entire volume of the cylinder.

3.2. *Concentration measurements*

Brown–Rebollo aspirating, hot-wire probes, sketched in figure 4 (Brown & Rebollo 1972), were used to measure the helium concentration fluctuations in the cylindrical volume during and after gas injection. Helium and helium/argon mixtures were used for the injected gases as they provided for a significant change in the thermal conductivity and specific heat of the air initially in the volume, and the probes were most sensitive to these properties. The probes are normally sensitive only to the thermodynamic properties of the gas flowing past the hot wire, as long as the Mach number of the external velocity field is much less than unity. However, at the level of sensitivity required for this study (concentration fluctuations of a few percent), the probes proved to be sensitive to the velocity fluctuations induced by the injection process. The 3 mm diameter probes were consequently shrouded with a short extension which was filled with acoustic foam (figure 4). The shroud length was adjusted until no signal could be detected when air was injected into the volumes. The shrouds increased the probe response time from a few ms to about 0.3 s. This

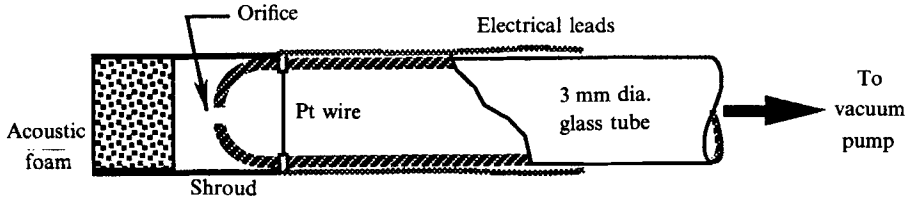

FIGURE 4. Sketch of shrouded Brown–Rebollo aspirating hot-wire probe.

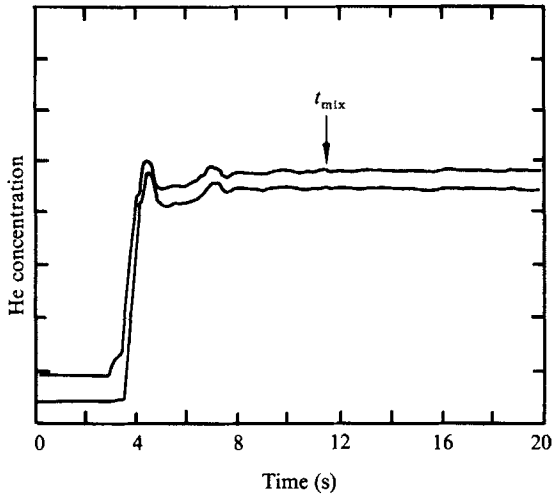

FIGURE 5. Typical double-probe signals.

long response time was nevertheless adequate to detect the relatively low-frequency fluctuations at the end of the mixing time in our large diameter tubes. The spatial resolution was estimated to be about 1 mm.

A pair of closely spaced Brown–Rebollo probes sampled the fluid at one of three locations within the cylindrical volume: top, side and bottom, $\frac{1}{4}D$ in from the wall and between two nozzles centrally located along the length of the volume. No significant differences were noted for the three locations. Two probes were used so that their signals could be correlated to help remove the deleterious effects of probe noise and drift.

Typical traces of the output of the probes as a function of time are shown in figure 5. The helium concentration rises irregularly with time, and the fluctuations eventually decline as the fluid is mixed to the new composition. The indicated concentration fluctuation level at which we chose to consider the fluid 'mixed' was arbitrarily set at $c'/\bar{c} = 0.025$, high enough to be above the probe noise yet low enough that the fluid had achieved approximate uniformity. This instant is indicated by the arrow in figure 5.

The results of the experiments are shown in figure 6. They are presented in terms of the dimensionless times, normalized by the characteristic time of equation (13). The general collapse of the data is a good indication of the validity of the model. The two curves shown in figure 6 are from (14) with the constants $K_4 = 80$ and $K_5 = 5$. Although there is considerable scatter for short-pulse injection, the data follow the general trend of the theory in the two limits. Note that the restriction that $\tau_j \ll 1$ for the short injection regime is overly conservative.

In order to confirm that the fluid motions were determined solely by the

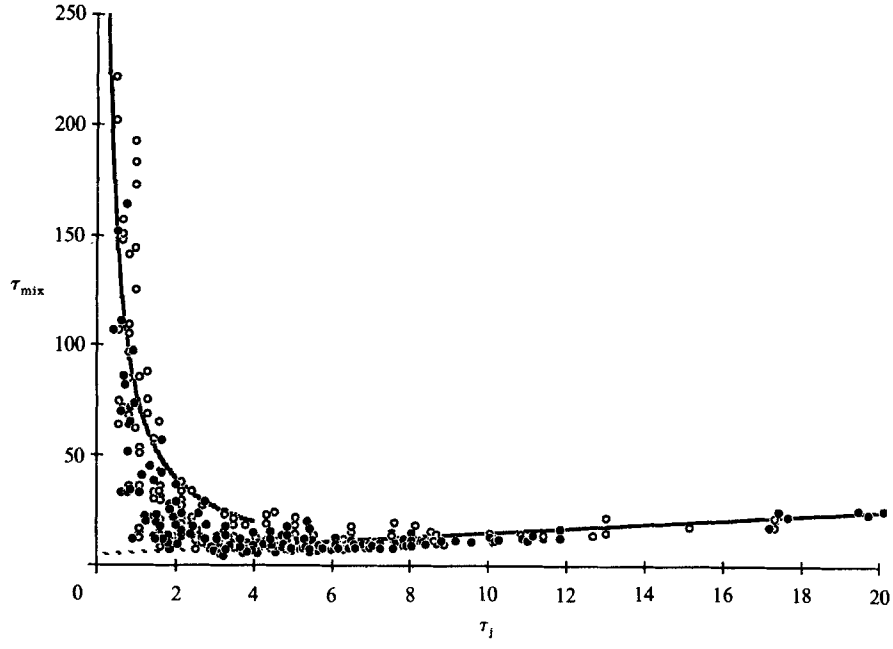

FIGURE 6. Experimental results and comparison with theory: ●, $D = 91$ cm; ○, $D = 61$ cm. Lines are from equation (14).

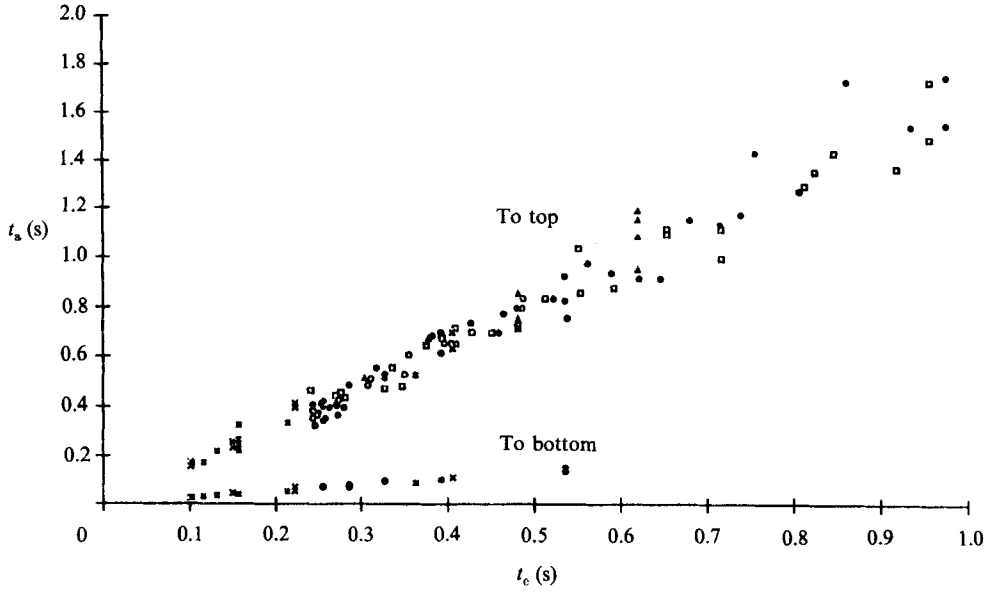

FIGURE 7. Arrival time of the injected fluid to the bottom and the top of the cylinder in the long-pulse limit.

parameters given in (7) and (9) in the two respective limits, the arrival times of the injected fluid at the bottom and the top of the mixing chamber were measured as a function of the injection parameters using both bare hot wires and unshrouded Brown–Rebollo probes. Figure 7 shows that the arrival times t_a at the bottom and the top are both proportional to the characteristic time; for this data set $t_j \geqslant t_c$.

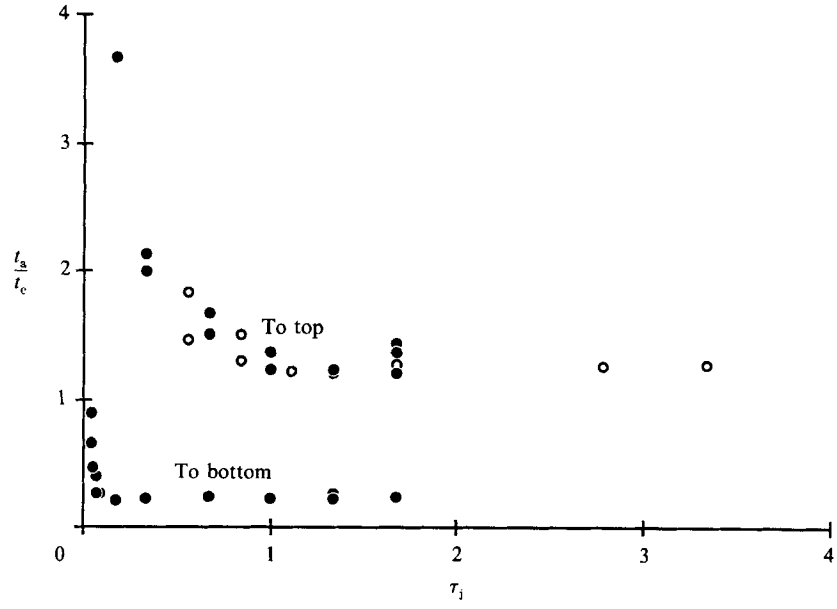

FIGURE 8. Dimensionless arrival time of the injected fluid to the bottom and top of the cylinder: ●, $D = 91$ cm; ○, $D = 61$ cm.

Figure 8 reveals that the arrival time is proportional to t_c only for sufficiently large τ_j; the transition occurring at larger values of t_j for arrival at the top compared to arrival at the bottom of the cylinder. Note that the transition occurs at about $\tau_j = 1$ for arrival at the top, where the vortices have grown to nearly fill the cylinder. For all of these experiments, the injection was sufficiently vigorous that buoyancy effects were small.

The magnitude of the scatter in the dimensionless mixing time (figure 6) at low values of the abscissa cannot be explained by experimental error. In some cases the experimentally observed mixing time varied by almost an order of magnitude when a run was repeated. One possibility is that the scatter reflects the spatial fluctuations in the concentration field, either throughout the volume or from the boundary layers. We note that the scatter is diminished in the long-pulse regime, an observation consistent with either possibility. In that regime, the steady jet may be less sensitive to any residual swirl. Also the vortices from the steady jet make many rotations before the jets are switched off. All the injected fluid except that which is injected near the end of the pulse has had many vortex rotations in which to mix. Therefore $c'/\bar{c}$ might be more spatially uniform. Also, the boundary layers would be more thoroughly flushed in the long-pulse regime. Further experiments will be required to identify the precise cause of the scatter.

4. Minimum mixing time

The above analysis and experiments show that the dimensionless mixing time, τ_{mix}, is a unique function of the dimensionless injection time, τ_j, and that this function displays a broad minimum at $\tau_j \approx 4$, is inversely proportional to τ_j for $\tau_j < 4$, and is proportional to τ_j for $\tau_j > 4$. This unique dependence can be used to determine the minimum mixing time, given a particular set of constraints. The remainder of this section is a simple demonstration of how this can be done.

For combustion applications, it is typical to fix the chamber diameter and final gas composition. To proceed, we choose to specify the mass fraction, β, of injected gas desired in the final gas mixture, which is given by

$$\beta = \frac{\dot{m} t_j}{\frac{1}{4}\pi \rho_f D^2}, \tag{17}$$

where ρ_f is the final density of the gas mixture and $\dot{m}$ is the injected mass flow rate per unit length. For simplicity, but without loss of generality, we assume that the injection orifice nozzles are choked and pressure matched. Then the jet thrust per unit span is $\dot{m}a^*$, where a^* is the choked speed of sound of the injected gas. The expression for the characteristic time, (13), becomes

$$t_c = \left(\frac{\rho D^3}{\dot{m} a^*}\right)^{\frac{1}{2}}. \tag{18}$$

Combining (17) and (18) results in a simple relationship between t_c and t_j:

$$t_c^2 = C_g D t_j, \tag{19}$$

where C_g is the gas composition parameter defined to be

$$C_g \equiv \frac{4\rho}{\pi \rho_f a^* \beta}. \tag{20}$$

Equation (19) indicates that the relationship between t_c and t_j is determined by the cylinder diameter D and the gases being mixed, with a weak dependence on temperature through the sound speed a^*. We can now proceed to solve for the minimum mixing time, given a final desired gas mixture and volume diameter; i.e. holding C_g and D constant. Application of (19) with (14) and (15) gives

$$\frac{t_{mix}}{C_g D} = \begin{cases} K_4, & \left(\dfrac{t_j}{C_g D}\right)^2 \ll 1, \\ \left(\dfrac{t_j}{C_g D}\right) + K_5 \left(\dfrac{t_j}{C_g D}\right)^{\frac{1}{2}}, & \left(\dfrac{t_j}{C_g D}\right)^2 \gg 1. \end{cases} \tag{21}$$

This equation is equivalent to normalizing time by a characteristic short injection time equal to $1/\Omega_s$. The data are replotted in this format in figure 9. The lines are calculated using $K_4 = 40$ and $K_5 = 5$. (Note that the value of K_4 was changed from 80 in figure 6, to 40 in order to provide a better fit to the data displayed in the format of figure 9 and figure 10 below.) Figure 9 shows that the minimum mixing time $\approx 40 C_g D$. Theoretically, this minimum mixing time is independent of the injection time in the short-pulse regime; however, as a practical matter, to avoid large variations in the mixing time (indicated by the large scatter in the data for the lower values of t_j), the optimal injection time is taken to be $16 C_g D$. The corresponding optimal characteristic time is given by $4 C_g D$. Knowing the characteristic time, the optimal gas injection system can then be designed. To summarize: the optimal conditions (denoted by $\hat{}$) for minimizing the mixing time for a pre-specified final gas mixture and cylindrical volume diameter are given by

$$\hat{t}_c = 4 C_g D, \tag{22}$$

$$\hat{t}_j = 16 C_g D, \tag{23}$$

$$\hat{t}_{mix} = 40 C_g D. \tag{24}$$

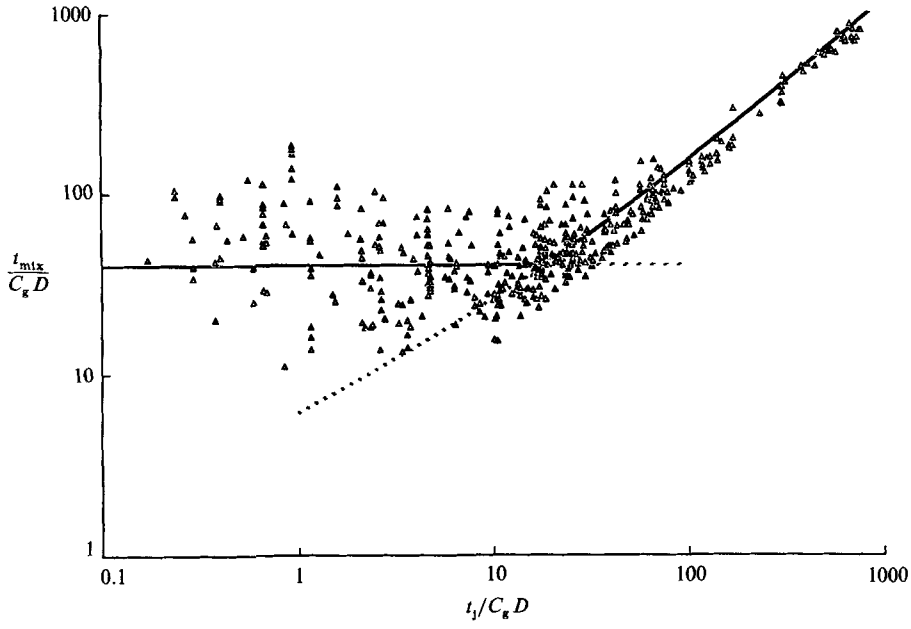

FIGURE 9. Comparison of theory and experiment with $C_g D$ normalization.

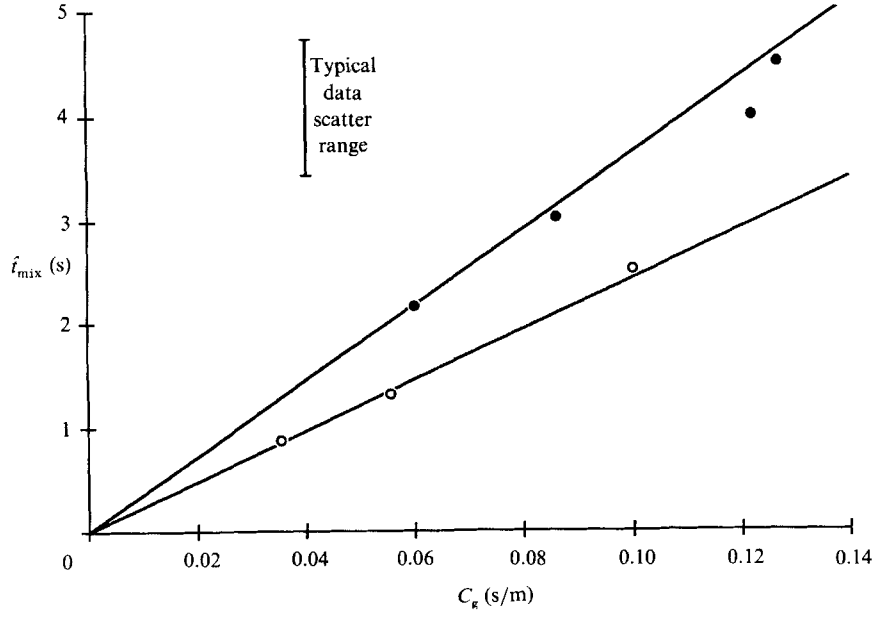

FIGURE 10. Explicit dependence of minimum mixing time, $\hat{t}_{mix}$, on composition parameter, C_g, and cylindrical volume diameter, D. Averaged data points: ●, $D = 91$ cm; ○, $D = 61$ cm; lines are from equation (24).

The most important result is that the minimum mixing time depends only on the final mixture composition and the cylinder diameter D to the first power. One might have expected the diameter dependency to follow one of the characteristic rotation times, which go as D^3 and $D^{\frac{3}{2}}$ from (8) and (10) respectively, or as the volume per unit

length, which goes as D^2. Our result suggests that mixing in large cylinders can be much more rapid than might have been anticipated.

A plot of experimentally measured minimum mixing time, t_{mix}, as a function of C_g is shown in figure 10 for the two cylinder diameters investigated. The values for C_g are corrected for thrust effects due to either subsonic or sonic and overexpanded injection nozzles. The data points are averages of about 5 runs each, with the typical scatter from one run to another indicated by the extent of the vertical line. The straight lines represent (24). The data generally agree with the model, although a wider range in D would be desirable for a more rigorous test.

Conclusions

A simple model for gas species mixing in a circular cylinder via a row of transverse jets has been developed which considers only the largest-scale global motions of self-similar vorticity and turbulence. The fine-scale motions, while ultimately responsible for the mixing at the molecular level, are not the rate-limiting process, and can therefore be ignored. Faster mixing is therefore promoted by investing the energy of the jets in the large-scale motions. Because of the existence of an intrinsic characteristic time for the large-scale global motions, two limiting mixing regimes exist, depending on whether the gas injection time interval is much less or much greater than the characteristic time. The minimum mixing time is shown to depend linearly on the product of the cylinder diameter D and gas composition parameter C_g. Experimental results using a Brown–Rebollo aspirating probe are in accord with the model, and permit determination of the appropriate constants so that the model can be applied to practical mixing problems. The model can easily be modified for application to other volume geometries and injector configurations.

The authors would like to thank Los Alamos National Laboratory for suggesting the problem. The mixing apparatus was designed by Harley Mann and Bob Bardon. Glen Peterson helped in conducting the experiment and in optimizing the probe. David Dowling contributed useful comments on the manuscript. The schlieren photographs are courtesy of N. Roy Greiner and Richard Heaton of the Los Alamos National Laboratory.

REFERENCES

BREIDENTHAL, R. E. 1981 Structure in turbulent mixing layers and wakes using a chemical reaction. *J. Fluid Mech.* **109**, 1.

BREIDENTHAL, R. E., TONG, K.-O., WONG, G. S., HAMERQUIST, R. D. & LANDRY, P. B. 1986 Turbulent mixing in two-dimensional ducts with transverse jets. *AIAA J.* **24**, 1867.

BROADWELL, J. E. & BREIDENTHAL, R. E. 1982 A simple model of mixing and chemical reaction in a turbulent shear layer. *J. Fluid Mech.* **125**, 397.

BROADWELL, J. E. & BREIDENTHAL, R. E. 1984 Structure and mixing of a transverse jet in incompressible flow. *J. Fluid Mech.* **148**, 405.

BROADWELL, J. E. & MUNGAL, M. G. 1988 Molecular mixing and chemical reactions in turbulent shear layers. *22nd Symp. (Intl) on Combustion*, pp. 579–587. Combustion Institute.

BROWN, G. L. & REBOLLO, M. R. 1972 A small, fast response probe to measure composition of a binary gas mixture. *AIAA J.* **10**, 649.

DREILING, T. D. 1987 Pulsed DF and DF-CO_2 laser performance. *J. Appl. Phys.* **61**, 1688.

EDWARDS, A. C., SHERMAN, W. D. & BREIDENTHAL, R. E. 1985 Turbulent mixing in tubes with transverse injection. *AIChE J.* **31**, 516.

HARTUNG, H. K. & HIBY, J. W. 1972 Beschleunigung der turbulenten Mischung in Rohren. *Chem. Ing. Tech.* **18**, 1051.

HILL, J. C. 1976 Homogeneous turbulent mixing with chemical reaction. *Ann. Rev. Fluid Mech.* **8**, 135.

KONRAD, J. H. 1976 An experimental investigation of mixing in two-dimensional turbulent shear flows with applications to diffusion-controlled chemical reactions. Ph.D. thesis, California Institute of Technology; and *Project SQUID Tech. Rep.* CIT-8-PU.

KOOCHESFAHANI, M. M. & DIMOTAKIS, P. E. 1986 Mixing and chemical reactions in a turbulent liquid mixing layer. *J. Fluid Mech.* **170**, 83.

MARBLE, F. E. & BROADWELL, J. E. 1977 The coherent flame model for turbulent chemical reactions. *Project SQUID Rep.* TRW 29314-6001-RU-00.